ELSEVIER

Journal of Atmospheric and Solar-Terrestrial Physics 70 (2008) 1012–1024

Journal of ATMOSPHERIC AND SOLAR-TERRESTRIAL PHYSICS

www.elsevier.com/locate/jastp

The Medieval and Modern Maximum solar activity imprints in tree ring data from Chile and stable isotope records from Antarctica and Peru

Nivaor Rodolfo Rigozo[a,b,c,*], Heitor Evangelista da Silva[b], Daniel Jean Roger Nordemann[c], Ezequiel Echer[c], Mariza Pereira de Souza Echer[a,c], Alan Prestes[d]

[a]*FAETEC—Faculdade de Educação e Tecnologia Thereza Porto Marques, Jacareí, SP, CEP 12308-320, Brazil*

[b]*LARAMG—Laboratório de Radioecologia e Mudanças Globais, Departamento de Biofísica e Biometria da Universidade do Estado do Rio de Janeiro, Pavilhão Haroldo Lisboa da Cunha, Subsolo, Rua São Francisco Xavier, 524, Maracanã, Rio de Janeiro, RJ, CEP 20550-013, Brazil*

[c]*INPE—Instituto Nacional de Pesquisas Espaciais, Av. dos Astronautas 1758, Cx. Postal 515, São José dos Campos, SP, CEP 12201-970, Brazil*

[d]*Universidade do Vale do Paraíba (UNIVAP), São José dos Campos, SP, Brazil*

Received 24 July 2007; received in revised form 26 December 2007; accepted 7 January 2008
Available online 12 January 2008

Abstract

This work presents a study of the relations between solar and climate variations during the last millennia by spectral and multi-resolution analysis for oxygen-18 and tree ring width time series. The spectral and wavelet analysis of tree ring data shows that main solar cycle periodicities are present in our time series at the 0.95 confidence level. This result suggests the possibility of a solar modulation of climate variations detected in accumulated ice oxygen-18. Results of spectral and wavelet analysis have shown that both solar and climate factors are also recorded in the oxygen-18 data.

Keywords: Solar–terrestrial relationships; Solar activity; Oxygen-18 time series; Spectral analysis; Multi-resolution analysis

1. Introduction

Dramatic variations such as sunspot numbers have been observed for more than a century in solar phenomena. Unambiguous confirmation of real variations in the Sun's radiation at the Earth is relatively recent: only during the past decade satellite measurements revealed the variability of the solar constant. During the last centuries, maxima and minima in solar activity have occurred approximately every 11 years. This is demonstrated clearly by sunspot data. The Sun also exhibits variability over time scales both longer and shorter than its dominant 11-year cycle (Hudson, 1988; Foukal, 1990).

The long-standing suggestion that variations in the Sun's total irradiance (the "solar constant") on

*Corresponding author at: FAETEC—Faculdade de Educaç ão e Tecnologia Thereza Porto Marques, Jacareí, SP, CEP 12308-320, Brazil. Tel.: +55 12 39456840; fax: +55 12 39456810.
E-mail address: rodolfo@faetec.br (N.R. Rigozo).

1364-6826/$ - see front matter © 2008 Elsevier Ltd. All rights reserved.
doi:10.1016/j.jastp.2008.01.002

time scales of decades to millennia may have been the cause of long-term climate variations has been revived in recent years by spacecraft radiometric measurements (Wilson and Hudson, 1988) showing that the Sun's total irradiance has varied more or less in phase with solar magnetic activity as measured by the sunspot number (SN) since the peak of solar cycle 21 in 1980. As was originally pointed out by Eddy (1976), the Maunder minimum coincided roughly with one of the Little Ice Age's coldest episodes when global temperatures were estimated as being 1–1.5 °C colder than modern temperatures (Corwley and Noth, 1991; Bradley and Jones, 1993).

The main solar activity mechanisms proposed to explain the imprint of the solar signal on the Earth's climate are (1) the variability of the total solar irradiance causing a change in the total energy input to the Earth's atmosphere and consequent warming/cooling (Solanki and Krivova, 2003); (2) the variability of the solar ultraviolet emission and its effects on the stratospheric ozone and thermal structure (Cubasch and Voss, 2000; Lean and Rind, 2001; Haigh, 2003). (3) The cosmic rays effects on the cloud coverage (Svensmark and Friis Christensen, 1997; Marsh and Svensmark, 2000; Carslaw et al., 2002; Harrison and Carslaw, 2003); Recently, a correlation between the global average of low cloud cover and the flux of galactic cosmic rays incident in the atmosphere has been observed (Svensmark and Friis Christensen, 1997). (4) High-energy particle precipitation effects on mesospheric and stratospheric ozone and thermal structure (Jackman et al., 2005; Vieira and da Silva, 2006). Whilst ozone changes in radiative forcing, energetic particles and cosmic rays have all been suggested to link solar changes with climate, they are by no means alternative explanations. It is quite conceivable that all could occur, but to different extents in different regions.

The proxy records of climate change and solar variability (obtained from ice cores and tree rings) can help find an answer to these Sun–climate relationships. Isotopic proxy series obtained from ice cores have been demonstrated to provide reliable information on historical climate variability. The higher accumulation rates in Dronning Maud Land in Antarctica (Graf et al., 2002) and Quelccaya ice cap in Southern Peru (Thompson et al., 1985) allow a more detailed record over the last glacial cycle. Tree ring thickness represents records of chronological series that are witnesses of the environment and climate that influenced their growth in the past (Fritts, 1976). Tree growth that lasts from birth to death is influenced by several simultaneous environmental factors: solar radiation, temperature, water precipitation and soil content, humidity, nutrients, neighborhood, pests, illness, etc. Depending on conditions and species, some of theses factors may prevail. The thickness variation of yearly rings reflects the tree sensitivity and the environmental factors at the place where it grows (Fritts, 1976). Thus, it may be thought that variations in the total irradiation from the Sun can induce variations in stable isotope content and in tree ring growth by some mechanisms that involve Sun-induced global and regional climatic variations.

The purpose of this paper study is to investigate the solar signal in ice core and tree ring proxies time series in epochs of the solar maximum (Medieval Maximum, 1140–1200, and Modern Maximum, 1900–1999). The study described in this article is based on a mathematical analysis of the time series of growth rings of trees sampled from Chile and of ^{18}O content of shallow firn and ice core from Dronning Maud Land in Antarctica and Quelccaya ice cap in Southern Peru. Characteristic features of the tree ring thickness variations and ice core ^{18}O content such as periodicities, trends and events are studied in order to obtain a greater understanding of the effects of solar activity on South America and Antarctica continents. The method used includes spectral analysis by iterative regression and wavelet analysis. The reasons for analyzing these proxy time series are (1) their lengths, which are much longer than instrumental records, (2) their high-frequency sampling rate, which is close to 1 year for the last 1000 years.

2. Data and analysis methods

In this work were used the following proxies: (1) the ^{18}O content ice core from Quelccaya ice cap in Southern Peru, lat.: 13°56′S, long.: 70°50′W, altitude: 5670 m (Fig. 1A) (Thompson et al., 1985). (2) The ^{18}O content of shallow firn and ice core from Dronning Maud Land in the Atlantic sector of Antarctica (Graf et al., 2002), lat.: 75°13′S, long.: 0°42′E, altitude: 2880 m (Fig. 1B). The data were obtained from PANGAEA—Publishing Network for Geoscientific & Environmental Data (www.pangaea.de). (3) Tree samples from Chile of *Fitzroya cupressoides* species (cypress tree, local name: alerce), collected at Costa del Osorno, lat.: 40°S, long.:

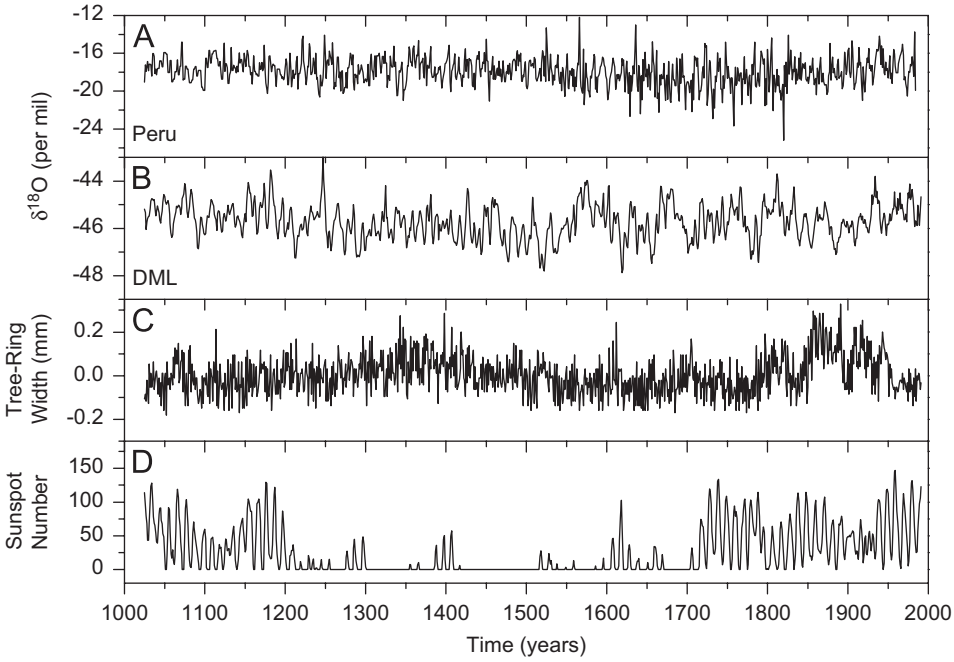

Fig. 1. $\delta^{18}O$ time series from Quelccaya, Peru (A). $\delta^{18}O$ time series from Dronning Maud Land (DML) in the Atlantic sector of Antarctica (B). Tree ring width from Osorno, Chile (C). Sunspot number time series (D).

73°50′W, altitude: 1000 m (Fig. 1C) (Nordemann et al., 2005). (4) The reconstruction SNs for the last 1000 years (Rigozo et al., 2001).

This study is made in the time interval between 1025–1202 and 1714–1984 that includes the Medieval and Modern Solar Maximum. The annual time series were analyzed by cross-correlation and iterative regression methods. These series were wavelet transformed using the orthonormal discrete Meyer wavelet transform. Using the wavelet analysis called multi-resolution analysis (or multi-level or multi-decomposition), cross-correlation analysis is performed between series 1 and series 2. A positive lag implies that series 1 maximum occurs after series 2 maximum and a negative lag implies that series 1 maximum occurs before series 2.

In this study, methods of spectral analysis by an iterative regression analysis (the ARIST "Análise por Regressão Iterativa de Séries Temporais"—Time Series Iterative Regression Analysis) were used to search periodicities present in time series. The ARIST method uses a simple sine function with three unknown parameters: a_0 = amplitude, a_1 = angular frequency and a_2 = phase (Wolberg, 1967; Rigozo and Nordemann, 1998). The starting point of the method is the definition of the so-called conditional function, which is

$$F = Y - a_0 \sin(a_1 t + a_2), \quad (1)$$

where Y is the signal (time series), t is time and a_0, a_1, a_2 are the three unknown parameters. For the determination of each parameter set, the maximum number of iterations used may be chosen between 50 and 200 (Rigozo and Nordemann, 1998). One of the main advantages of this method is that it gives the standard deviation of every determined parameter. This allows a selection of the most important amplitudes (when amplitude >2 standard deviations (SD), 95% confidence level), which present a greater value of the amplitude/deviation ratio.

The wavelet transform is a very powerful tool to analyze non-stationary signals. It permits the identification of main periodicities in a time series and the evolution in time of each frequency (Kumar and Foufoula-Georgiou, 1997; Torrence and Compo, 1998; Percival and Walden, 2000). The wavelet transform of a discrete data series is defined as the convolution between the data series with a scaled and translated version of the wavelet function chosen. By varying the wavelet scale and translating in time, it is possible to construct a picture showing

the amplitude of any characteristic versus scale and how this amplitude varies with time.

In this work, the complex Morlet wavelet analysis was used because it is the most adequate to detect variations in the periodicities of geophysical signals in a continuous way along time scales. The Morlet wavelet is a plane wave modulated by a Gaussian function (Torrence and Compo, 1998; Percival and Walden, 2000):

$$\psi(0)_{\eta} = \pi^{-1/4} e^{iw_o\eta} e^{-\eta^2/2}. \quad (2)$$

The wavelet transform may be continuous or discrete. Digitized data analysis by computer processing evidently has to be discrete. Thus the difference is that the continuous wavelet transform (CWT) decomposes a signal in 2^j levels, these levels can be constituted by every frequency, i.e. j can be a fractionary power. On the other hand, the discrete wavelet transform (DWT) operates only on the integer powers of j.

While the CWT works with time series defined over the entire real axis, the DWT deals with series defined essentially over a range of integers ($t = 0, 1,\ldots,N-1$), where N is the number of values in the time series. Thus, a time series $x(t)$ has N data points. The DWT$\{x\}$ will also have N points or N coefficients. The 2^{j-1} scales are the wavelet coefficients and 2^j, the last scale, is the scaling coefficient. Each 2^{j-1} scale has $N_j = N/2^j$ wavelet coefficients (the number of coefficients reduces with scale). The wavelet coefficients are proportional to the difference of averages. The scaling coefficient is proportional to the averages of the original data and reflects long-term variations. The sub-sampling of the DWT collapses the two-dimensional CWT back into a one-dimensional quantity. For most series it is interesting to perform the analysis by using a less coarse sampling in time, i.e. consider sub-samples of the CWT that preserve some of its redundancy. The maximum overlap discrete wavelet transform (MODWT) is a sub-sampling of the CWT at dyadic scales, but in contrast to the DWT, we now deal with all times t and not just those that are multiples of 2^j. Each scale has the same number of coefficients (Percival and Walden, 2000).

The MODWT may be used in multi-resolution analysis (MRA) or wavelet decomposition analysis, which is concerned with the study of signals or processes represented at different resolutions and developing an efficient mechanism to going from

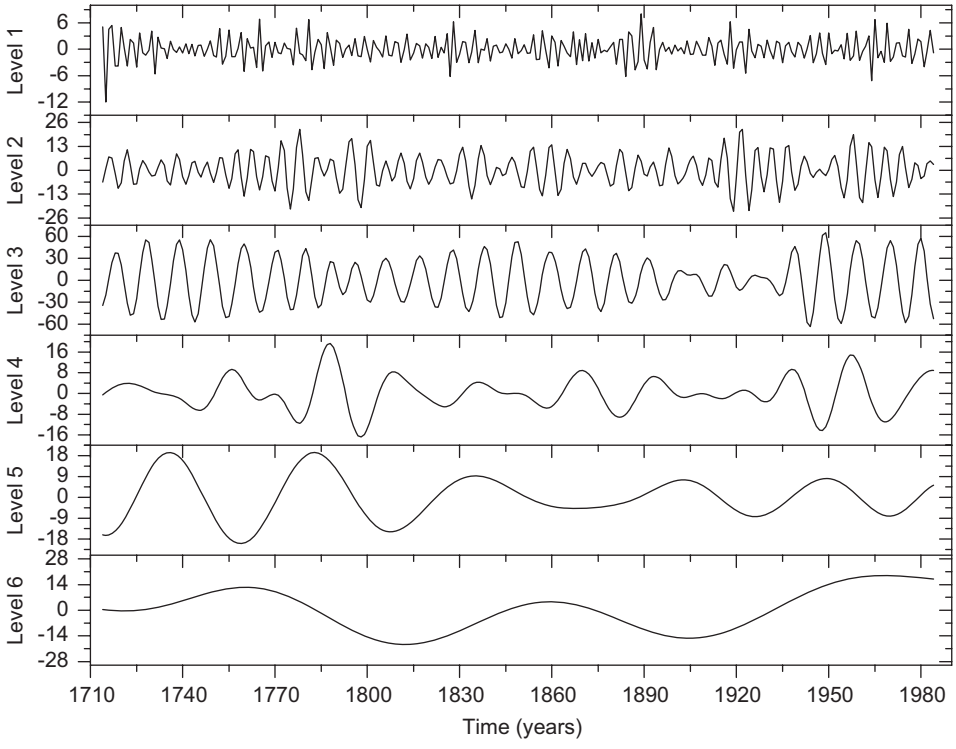

Fig. 2. Wavelet decomposition bands for the sunspot number (SN) time series (1714–1984).

one resolution to another (Kumar and Foufoula-Georgiou, 1997; Percival and Walden, 2000; Echer, 2004; Echer et al., 2004). In the MRA, a signal S is decomposed in an approximation A and in a detail D. The detail contains the high-frequency part of the signal, whereas the approximation contains most of the characteristic frequencies of the signal. In the first step of the decomposition, $S = A_1 + D_1$. In a next step, the approximation itself is split in a second-level approximation, $A_1 = A_2 + D_2$, and $S = A2 + D_2 + D_1$, and the process continues as shown in Fig. 2. The A and D levels can be seen as low-pass and high-pass band filters. Further, as in each decomposition the higher frequency part of signal was put in a D_{j-1} level, the new D_j level can be seen as a band pass filter, containing frequencies lower than the ones present in the D_{j-1} level and higher than the ones in the A_j level as shown Fig. 2 (to the SN for example).

3. Results and discussion

The spectral analysis results in δ^{18}O-Peru, δ^{18}O-DML, tree ring width and SN time series are described. Figs. 3E–H and 4E–H show the amplitude spectra as a function of frequency as determined by the ARIST method. It may be observed in the spectrum that there is no domination of long periods over the short ones, or, in other terms, the long periods do not hide the low periods in the spectrum. The nature of this distribution suggests a favorable response in ^{18}O contents and tree ring to environmental factors for short and long periods. The periods indicated are significant at the 95% confidence level (amplitude $> 2 \times$ SD).

It may be observed that the periodicities found, in four time series, for the Medieval and Modern Maximum solar are practically the same ones (Figs. 3 and 4E–H). Some differences occur mainly

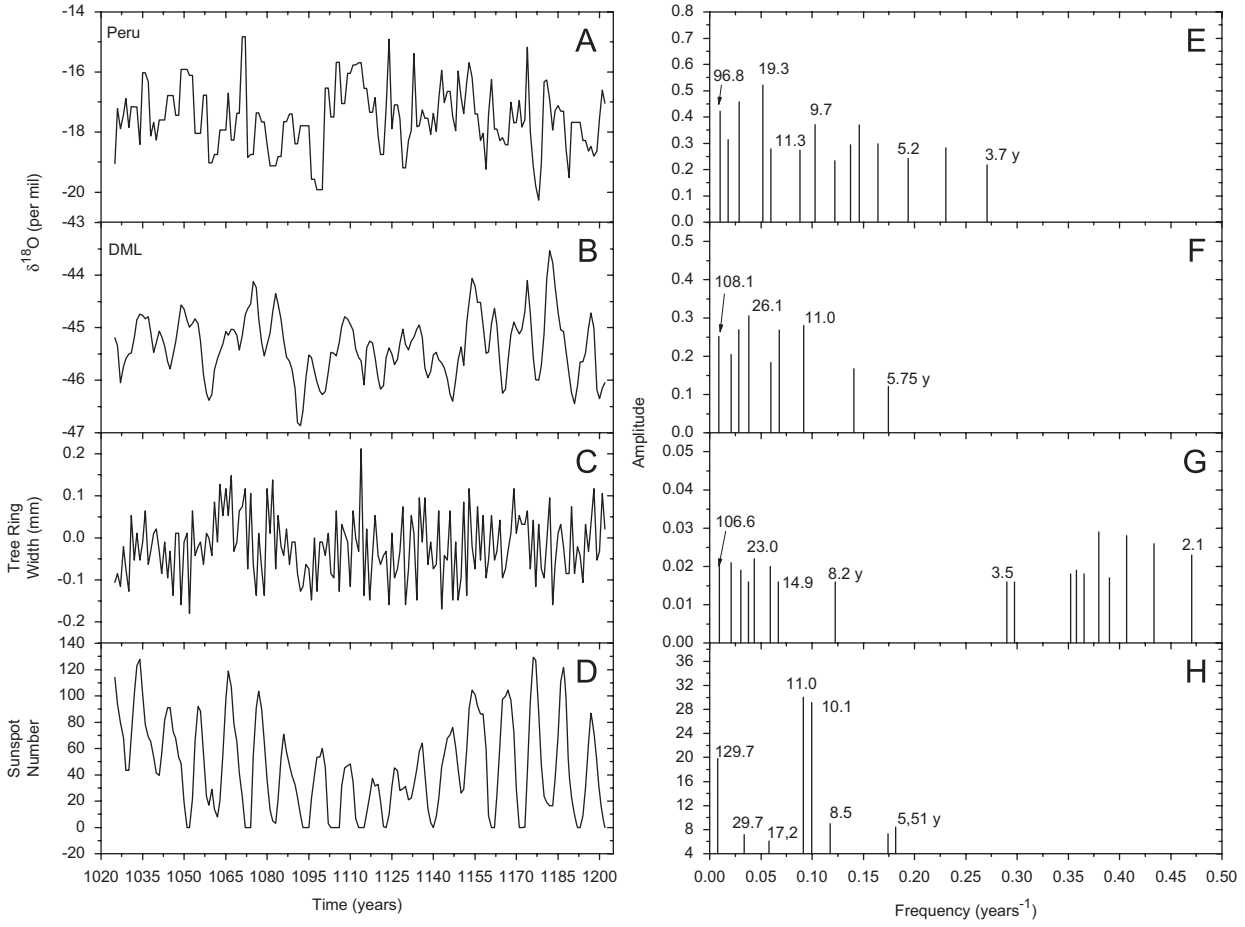

Fig. 3. Time series for interval time 1025–1202 (A–D). Amplitude spectrum to δ^{18}O-Peru (E), δ^{18}O-DML (F), tree ring width (G) and sunspot number (H).

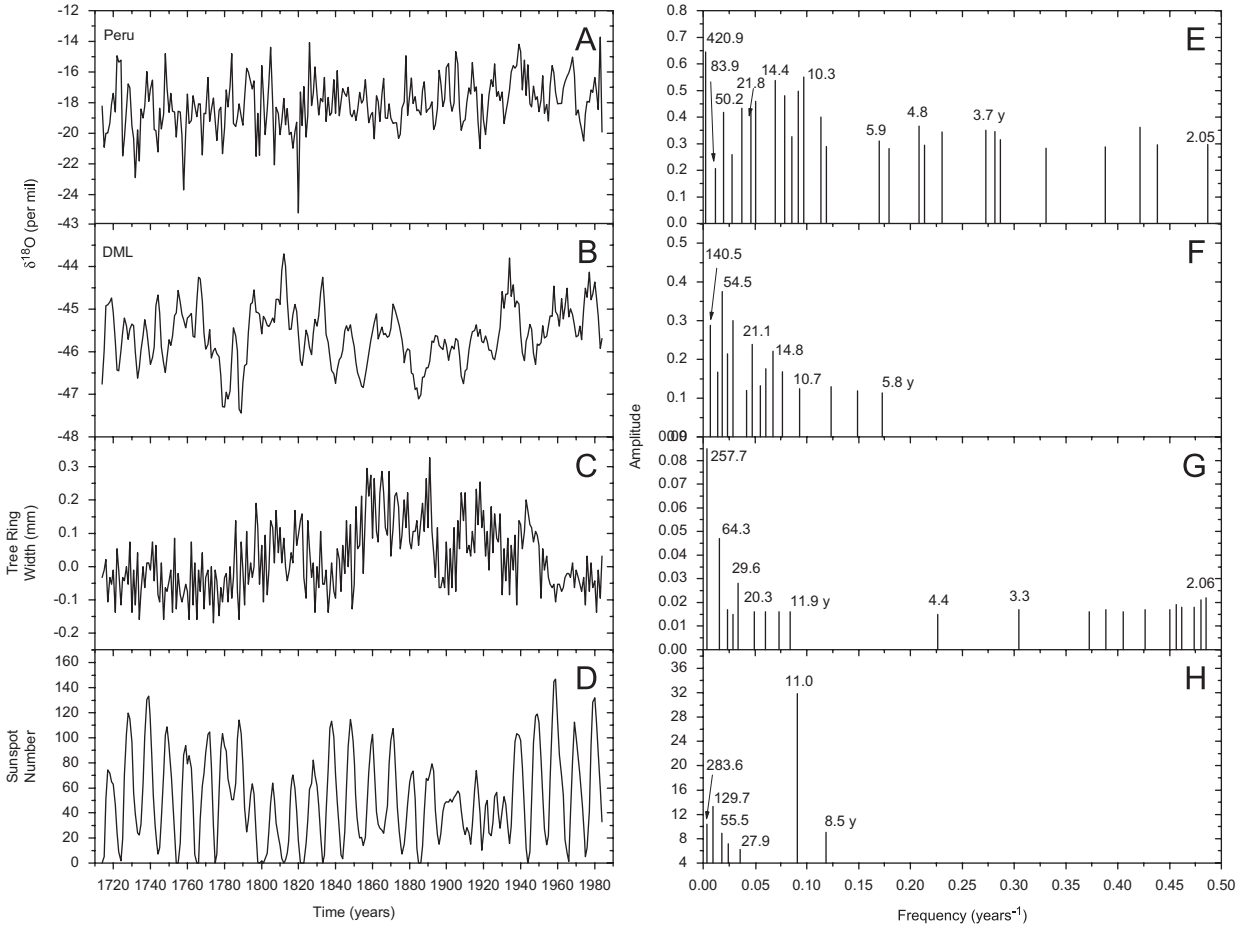

Fig. 4. Time series for interval time 1714–1984 (A–D). Amplitude spectrum of δ^{18}O-Peru (E), δ^{18}O-DML (F), tree ring width (G) and sunspot number (H).

in the long periods, where they appear in the interval of the Modern Maximum and do not appear in the Medieval Maximum interval. The solar signals at 11, 22 and 80 years are found in proxies for the two periods of the Modern and Medieval Maximum.

The periodicities found by us, in δ^{18}O time series, are in accordance with the studies of profiles of ^{18}O in foraminifers, made by Cini Castagnoli et al. (1999), who have found evidence of the influence of the solar activity at 11.4 years. Johnsen et al. (1970) and Dansgaard et al. (1971) studying the ^{18}O contents in ice core from Camp Century (Northwest Greenland) had found two significant peaks at 78 and 181 years, which they attributed to possible solar changes.

The periodicities found by us, in tree ring time series, are in agreement with studies made by Nordemann et al. (2005), in which they studied tree rings from Concordia, Brazil (1797–1996), and from Osorno, Chile (564 BC–1991 AD), where they find periodicities of 5.5, 11, 22, 50 and 89 referred to solar cycles. Rigozo et al. (2006) studying tree ring time series from Pious XI, Chile (1994–1587), found periodicities of 5.5, 11.9, 21.8 and 99.1 years referred also to solar cycles.

After the verification of a possible presence of periodicities of the solar variability, now a comparative study is made between δ^{18}O-Peru × SN, δ^{18}O-DML × SN and tree ring × SN, for 1025–1202 and 1714–1984, which is made to verify the response of proxies as a function of solar signals. This will be made through the cross-correlation and MRA.

The cross-correlation coefficients, with lag 0, were calculated among these variables: δ^{18}O-Peru × SN: −0.14; δ^{18}O-DML × SN: 0.16 and tree ring × SN: −0.01 for 1025–1202, and δ^{18}O-Peru × SN: 0.11; δ^{18}O-DML × SN: −0.06 and tree ring × SN: −0.14 for 1714–1984. One can see that in all cases the

significance is low. This occurs due to local conditions being predominant in the variation of proxy time series.

3.1. Decomposition

Thus, the MRA was performed in the four time series in order to study the dependence of ^{18}O on SN and of tree ring on SN and its variations on different timescales. The decomposition was performed until the D_5 level. The D_j levels and the A_6 approximations for SN time series are shown in Fig. 2. The band frequencies are approximately D_1 (2–4 years), D_2 (4–8 years), D_3 (8–16 years), D_4 (16–32 years) and D_5 (32–64 years). A_6 is the scaling level, corresponding to the long-term periods (>64 years). Echer et al. (2004) utilized this technique for the A_a index reconstruction and obtained a high correlation between the original time series and the reconstructed time series of 0.91.

D_1 and D_2 levels correspond to the high-frequency oscillations, from the Nyquist cutoff frequency (2 years) to the 4 years, for D_1. It is hard to see any pattern in this high-frequency, highly noisy band. The cross-correlations were performed in these levels and the correlation coefficients are very low (Tables 1 and 2). The spectral analysis of these levels for the $\delta^{18}O$ and tree ring presents some different periodicities, for the same decomposition level in the SN. Thus, the correlation between $\delta^{18}O \times SN$ and tree ring SN, to D_2, only in the period found close to 5 years, which corresponds to the maximum in each signal. The cross-correlation coefficients found are shown in Tables 3 and 4.

The D_3 and D_4 levels encompass the 11- and 22-year solar cycle. The correlation between $\delta^{18}O \times SN$ is better for 1025–1202 (Table 1) than for 1714–1984 (Table 2). The correlation between tree ring and SN is high only for the D_4 level for 1025–1202 (Table 1). The spectral analysis of these levels for the $\delta^{18}O$ and tree ring presents some different periodicities, for the same decomposition level in the SN. This should explain the low correlation between them. Thus, the correlation between $\delta^{18}O \times SN$ and tree ring SN, of D_3 and D_4 levels, only obtained in the period found in SN (10, 11 and 22 years), $\delta^{18}O$ (10, 11 and 21 years) and tree ring (11 and 22 years), corresponds to the maximum in each signal. The cross-correlation coefficients found are shown in Tables 3 and 4.

The D_5 level corresponds to the band frequency 32–64 years and presents a better correlation for $\delta^{18}O$-DML $\times$ SN than $\delta^{18}O$-Peru $\times$ SN and tree ring $\times$ SN for 1025–1202 (Table 1). The 1714–1984 period observed a high correlation between the $\delta^{18}O$-DML $\times$ SN and an increase of the correlation between tree ring $\times$ SN and $\delta^{18}O$-Peru $\times$ SN (Table 2) in relation to the period 1025–1202. The spectral analysis found two periods in proxies and one period in SN for 1714–1984 and two periods in

Table 1
Decomposition bands cross-correlations (lag −1 to 1) between sunspot number and proxies to 1024–1202

Level	SN × tree ring	SN × DML	SN × Peru
D_1	−0.1274	−0.1682	−0.1349
D_2	−0.1996	−0.1133	−0.0487
D_3	0.2736	−0.4166	−0.4406
D_4	0.6357	0.4962	0.0673
D_5	−0.0484	0.5070	0.1428
A_6	0.1425	0.8678	0.0753

Table 2
Decomposition band cross-correlations (lag −1 to 1) between sunspot number and proxies to 1714–1984

Level	SN × tree ring	SN × DML	SN × Peru
D_1	−0.1251	0.0669	0.0568
D_2	−0.1704	0.1215	0.1925
D_3	−0.0289	0.0391	0.2303
D_4	−0.3189	0.3758	0.0924
D_5	−0.5133	−0.8716	0.4307
A_6	−0.4416	0.3824	0.2418

Table 3
Solar proxy cross-correlations at medieval maximum

Level	SN × Chile	Lag	SN × DML	Lag	SN × Peru	Lag
D_2	−0.99	1	−0.87	2	−0.96	0
D_3	−0.98	1	−0.99	2	−0.90	3
D_4	0.77	2	0.99	2	0.98	3
D_5	–	–	0.80	1	0.90	1
A_6	0.87	9	0.98	5	0.66	−9

Table 4
Solar proxy cross-correlations at modern maximum

Level	SN × Chile	Lag	SN × DML	Lag	SN × Peru	Lag
D_2	0.61	0	−0.93	−1	0.96	−1
D_3	−0.52	0	−0.96	1	–	–
D_4	−0.90	0	0.90	1	0.92	2
D_5	−0.73	0	−0.91	0	0.75	0
A_6	−0.79	9	0.70	9	0.91	−9

SN, δ^{18}O Peru, δ^{18}O-DML and one period in tree ring for 1025–1202. The similar periodicity between them is of 52 years for 1714–1984. The cross-correlation coefficients found with lag 0 are shown in Table 4. However, for 1025–1202, the correlations exist only between the periods of δ^{18}O and SN with lag 1 year (Table 3).

Finally, the approximation level A_6 shows the long-term trends and the correlation in this level is high only between δ^{18}O-DML for 1025–1202 (Tables 1 and 2). A similar periodicity was found in proxies and SN close to 100 years, for the interval 1025–1202. The cross-correlations were performed in these levels and the correlation coefficients are high (Table 3). However, for 1714–1984, the similar periodicity found in proxies and SN is the next 200 years. The cross-correlations are also high (Table 4).

3.2. Reconstruction

It is possible to verify the behavior of the concentrations of the ^{18}O contents in the ice and of tree ring growth caused by solar activity variations. This is achieved through the reconstruction of these time series as a function of the solar signal, for the two time intervals 1025–1202 and 1714–1984. This reconstruction is made through the addition of all the periodicities found in all the levels by the ARIST method (since it determines the amplitude, frequency and phase). Periodicities of proxies present a relation with SN and this allows their reconstruction in function of the SN periodicities through a linear relation.

Thus, the reconstruction of proxies is made by the addition of periodicities found at each level with the periodicities close to 5.5, 11, 22, 33 (to 1025–1202), 52 (to 1714–1984) and 100 years (to 1025–1202) and long trend (for 1714–1984) being substituted by the linear relation between δ^{18}O-Peru × SN, δ^{18}O-DML × SN and tree ring × SN, respectively.

Fig. 5 shows the solar signal reconstruction in the δ^{18}O and the tree ring time series, for the interval 1025–1202. Fig. 6 already shows the reconstruction of the solar signals in the δ^{18}O and the tree ring time series, for 1714–1984. The correlation coefficients obtained between the original series (1025–1984) and reconstruction series (in function of SN) are 0.44 for the tree ring, 0.47 for δ^{18}O-DML and 0.23 for δ^{18}O-Peru. This represents a correlation of 0.19 (to 1025–1202) and 0.44 (to 1714–1984) for tree ring, 0.32 (to 1025–1984) and 0.52 (to 1714–1984) for δ^{18}O-DML and 0.27 (to 1025–1202) and 0.11 (to 1714–1984) for δ^{18}O-Peru, as shown in Table 5.

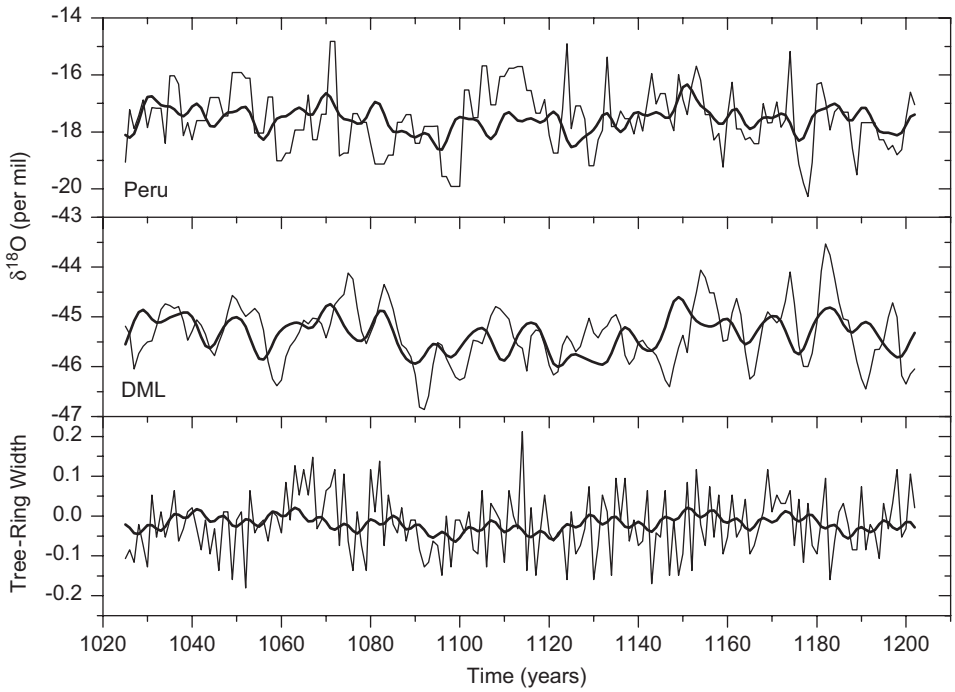

Fig. 5. Reconstruction of the solar signal in proxies for Medieval Maximum (hard line).

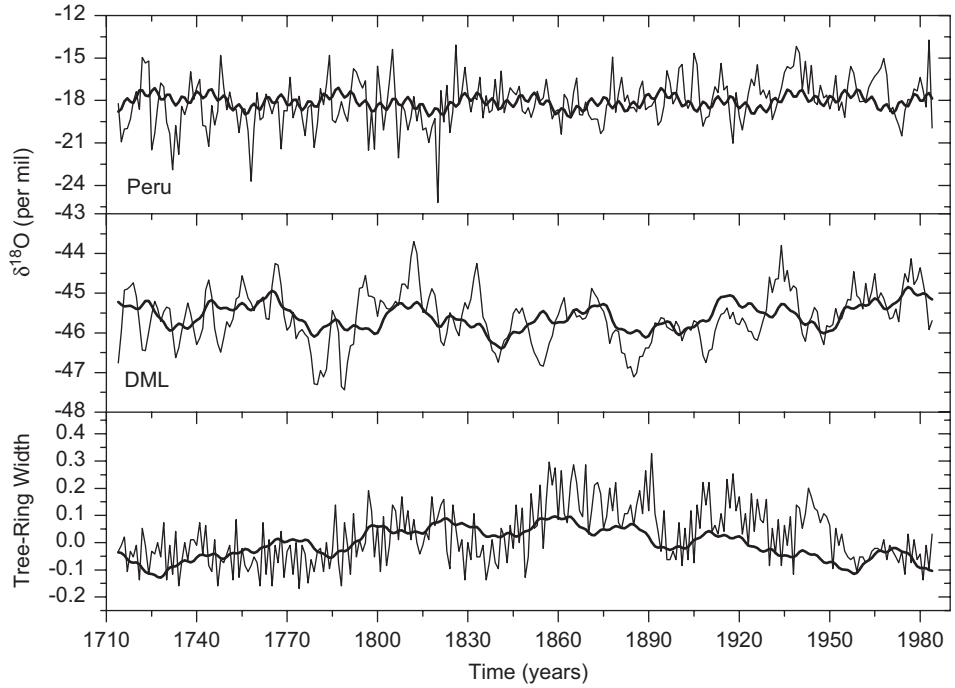

Fig. 6. Reconstruction of the solar signal in proxies for Modern Maximum (hard line).

Table 5
Cross-correlations between original proxies and reconstruction solar signal in proxies

Time (years)	Chile × Chile	DML × DML	Peru × Peru
1025–1984	0.44	0.47	0.23
1025–1202	0.19	0.32	0.27
1714–1984	0.44	0.52	0.11

The wavelet spectrum of $\delta^{18}O$ measured in Peru Andes shows the strongest feature and it is a persistent signal near the 22-year cycle during Medieval Maximum to 1037–1127 (Fig. 7A) and during the Modern Maximum it occurs with a major intensity during SN maximum intervals, after 1714–1774, 1804–1834, 1864–1894 and 1924–1984 (Fig. 8A). It is observed that the 22-year cycle presents a period variation with time to 17–33 years. The variability of the short period, 2–8 years, is more persistent in time for the Modern Maximum than that in the Medieval Maximum (Figs. 7A and 8A), presenting a period variation of 2–8 years. The 11-year cycle is persistent in time during the Medieval Maximum and Modern Maximum. It presents a period variation of 7 of the 17 years. Already the Gleisberg cycle is persistent in time with periodicity variations of 64–100 years during the Modern Maximum (Fig. 8A) and 64 years in the Medieval Maximum (Fig. 7A).

The wavelet spectrum of $\delta^{18}O$ measured in DML Antarctica shows a persistent signal near the 22-year cycle during Medieval Maximum (Fig. 7B) than that of the Modern Maximum (Fig. 8B), with a period variation with time to 17–33 years. In Modern Maximum the 22-year signal is present in 1774–1984 time intervals, with period variation close to 25 years (Fig. 8B). The variability of the short period, 2–8 years, is more sporadic in time for the Medieval and Modern Maximum (Figs. 7B and 8B), presenting a period variation of 4–8 years. The 11-year cycle consists of sporadic events during the Medieval Maximum and Modern Maximum. In Medieval Maximum two sporadic events occur to 1052–1112 and 1142–1202, with period variations of 8–17 years (Fig. 7B). The Gleisberg cycle is persistent in the time with periodicity variations of 60–100 years during the Modern Maximum (Fig. 8B) and 64 years in the Medieval Maximum (Fig. 7B).

Figs. 7C and 8C present a wavelet spectrum of tree ring width where it may be observed that the periodicity close to 22 years is more persistent in time during Medieval Maximum than that in Modern Maximum. In Medieval Maximum the

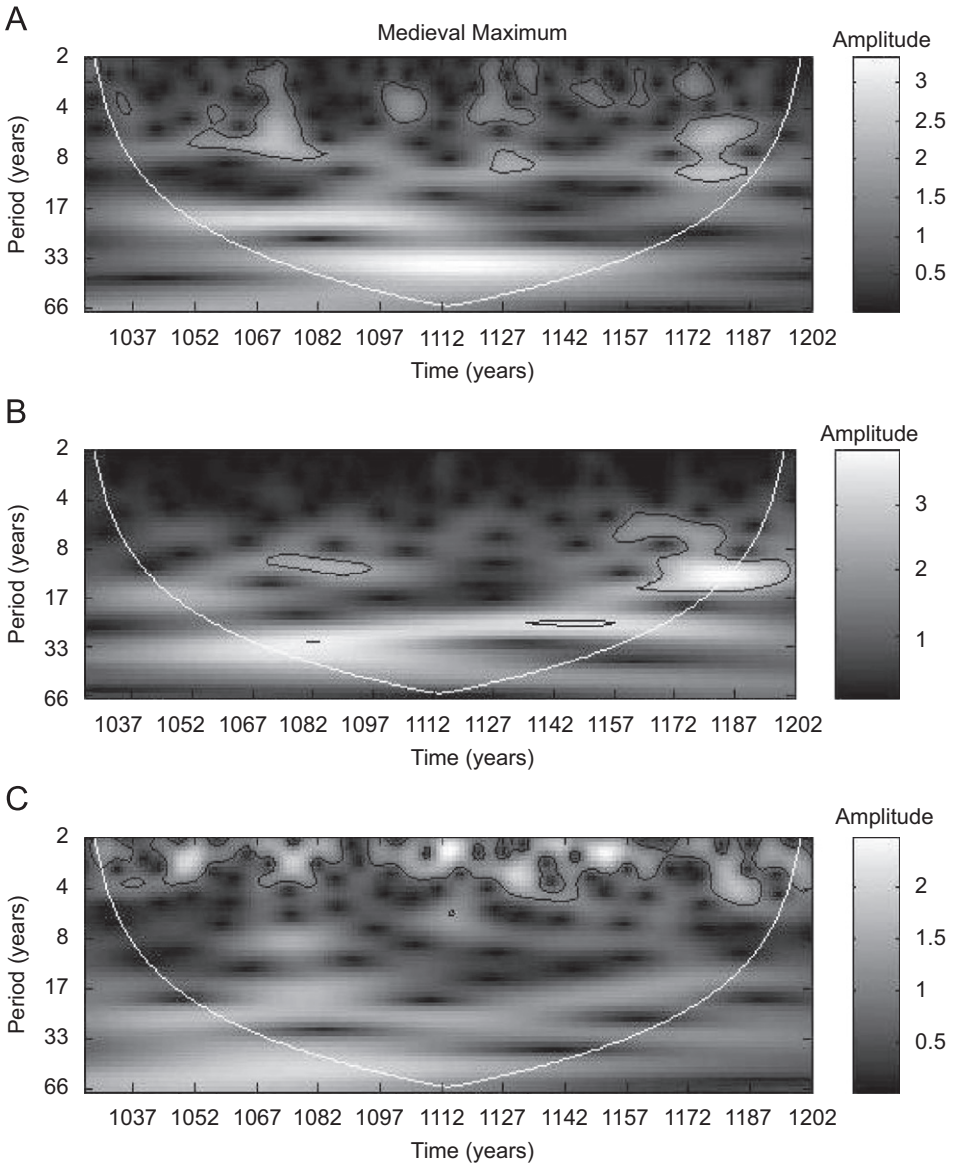

Fig. 7. Morlet spectrum of the δ^{18}O-Peru (A), δ^{18}O-DML (B), and tree ring width from Chile (C) for interval time 1025–1202, with cone of influence (parabolic curve), and significance levels contour for 95%. At right the legend indicates amplitude spectra scale in grayscale. *Y*-axis is the scale (period) in days, and *X*-axis is the time in years. The grayscale code indicates the amplitude spectra of each periodicity at a given time.

22-year cycle shows a period variation in time of 17–33 years (Fig. 7C). In Modern Maximum it presents one event between 1864 and 1828, with period variation close to 25 years (Fig. 8C). Also, the short periodicities between 2 and 8 years also present more significant persistent events in Medieval and Modern Maximum. The 11-year cycle presents sporadic events in time for Medieval and Modern Maximum. The Gleisberg cycle observed also shows a persistence event during Modern Maximum with period variation between 60 and 100 years (Fig. 8C), and during Medieval Maximum close to 64 years (Fig. 7C).

Note that solar activity periodicities can considerably deviate from their average values during different time intervals to Gleisberg, Hale and Schwabe solar cycles. Peristykh and Damon (1998) in their study about modulation of atmospheric ^{14}C

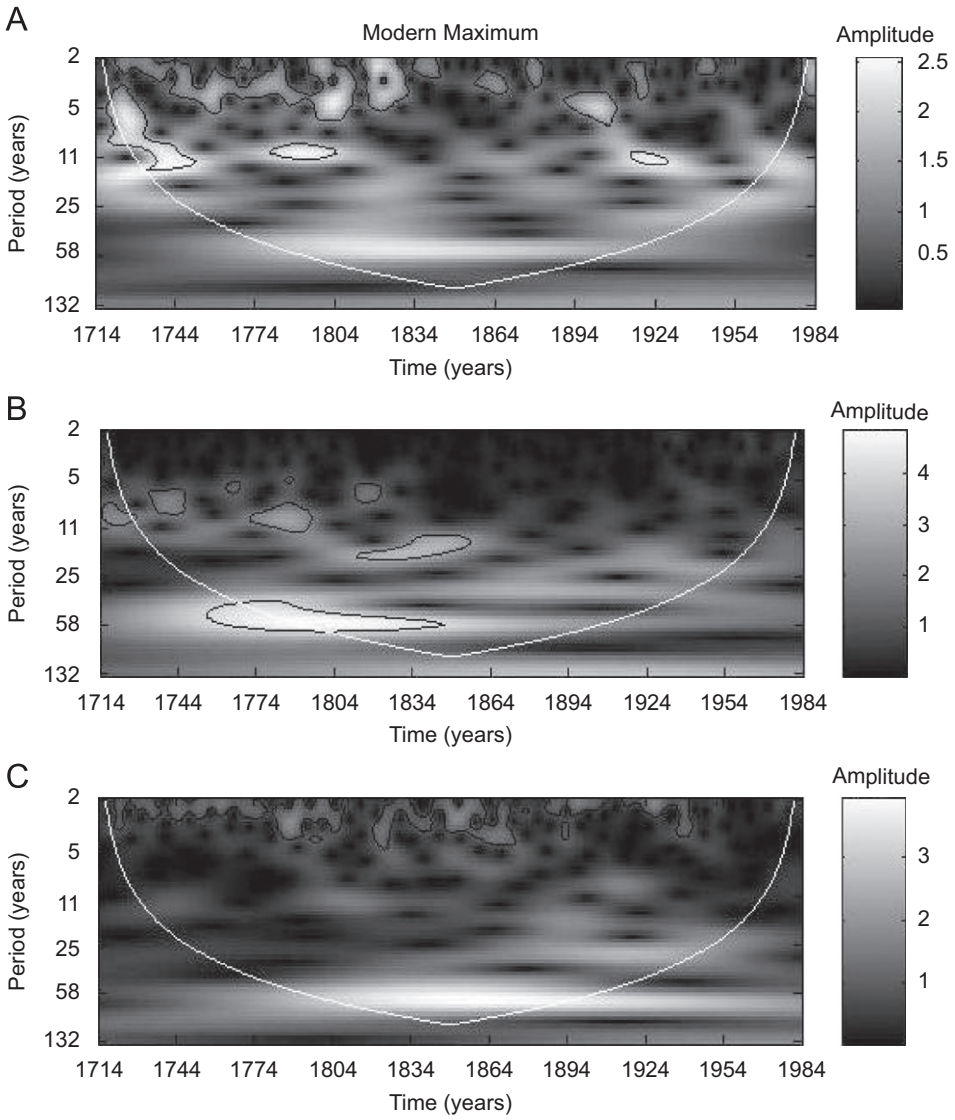

Fig. 8. Morlet spectrum of the δ^{18}O-Peru (A), δ^{18}O-DML (B) and tree ring width from Chile (C) for interval time 1714–1984, with cone of influence (parabolic curve) and significance levels contour for 95%. At right the legend indicates amplitude spectra scale in grayscale. *Y*-axis is the scale (period) in days, and *X*-axis is the time in years. The grayscale code indicates the amplitude spectra of each periodicity at a given time.

concentration by solar wind and irradiance components of Hale and Schwabe solar cycles and Raspopov et al. (2004) study the periodicity of climate conditions and solar variability derived from dendrochronological and other palaeoclimatic data in high latitudes, and have shown that during the time interval around the Maunder minimum of solar activity the period of the 22-year cycle varied from 22 to 26 years. In our work we observed that Medieval Maximum shows this variation in periodicities: Hale solar cycles, 22.9 ad 26.5 years (Chile tree ring data), 26.1 years (DML δ^{18}O) and 19.3 years (Peru δ^{18}O). In the Modern Maximum was observed 20.7 years (Chile tree-ring data), 21.1 and 23.9 years (DML δ^{18}O), and 19.7, 21.8 and 26.8 years (Peru δ^{18}O).

Figs. 7 and 8 show clearly that each proxy registers the environmental variations differently, whether they are caused by a climatic or solar forcing. Lean and Rind (1994) showed, in their model, that during Maunder Minimum epoch, the Earth presented different temperature variations for

each region of the planet, for a reduction in the solar irradiation. On the other hand, Vieira and da Silva (2006) showed in their study that the association of the cloud effects on the radiative fluxes in the atmosphere and the Southern Hemisphere Magnetic Anomaly (SHMA) gives rise to a new interpretation of the observed climate changes. As the SHMA is a dynamic feature of the Earth's magnetic field and is drifting westward, a westward drift of the cloud effects on the radiative flux is expected. The main consequence of the drift of the SHMA could be an increase in the area over the Pacific with an intense negative forcing that could increase the variability of the SST and atmospheric circulation associated with ENSO phenomena.

4. Conclusion

This result suggests a solar modulation in ice ^{18}O and in tree growth ring. The spectral analysis of tree rings and $\delta^{18}O$ data shows that the main periodicities of the solar cycle, 5.5, 11, 22, 50 and 80 years, were present in our time series at the 0.95 confidence level. Short-term variations, between 2 and 7 years, are also present.

Thus, we made a reconstruction of the solar signal for these proxies. The reconstruction of proxies is made by the addition of the periodicities found in each level, the periodicities close to 5.5, 11, 22, 33 (to 1025–1202), 52 (to 1714–1984), 100 years (to 1025–1202) and long trend (for 1714–1984) being substituted by the linear relation between $\delta^{18}O$-Peru $\times$ SN, $\delta^{18}O$-DML $\times$ SN and tree ring $\times$ SN, respectively. Through this reconstruction, by cross-correlation between the original and reconstruction time series, it may be evidenced that proxies have better response to the solar variability in the period of the Modern Maximum (1714–1984) than during the Medieval Maximum (1025–1202).

Acknowledgments

The authors would like to thank, for the support granted to this research, N.R. Rigozo-CNPq (APQ 470764/2006-6 and post-doctoral fellowship, 150211/2007-4) and M.P. Souza Echer FAPESP post-doctoral fellowship (2006/467-2), E. Echer-FAPESP research support project (2005-03501-4) and CNPq (PQ 300104/2005-7). Thanks to Publishing Network for $\delta^{18}O$ data from Geoscientific & Environmental Data (www.pangaea.de).

References

Bradley, R.S., Jones, P.D., 1993. 'Little Ice Age' summer temperature variations: their nature and relevance to recent global warming trends. The Holocene 3, 367–376.

Carslaw, K.S., et al., 2002. Cosmic rays, clouds, and climate. Science 298, 1732–1737.

Cini Castagnoli, G., Bonino, G., della Monica, P., Taricco, C., Bernasconi, S., 1999. Solar activity in the last millenium recorded in the ^{18}O prole of planktonic foraminifera of a shallow-water ionian sea core. Solar Physics 188, 191–202.

Corwley, T.J., Noth, G.R., 1991. Paleoclimatology. Oxford University Press, New York.

Cubasch, U., Voss, R., 2000. The influence of total solar irradiance on climate. Space Science Reviews 94, 185–198.

Dansgaard, W., Johnsen, S.J., Clausen, H.B., Langway Jr., C.C., 1971. Climatic record revealed by the Camp Century ice core. Late Cenozoic Glacial Ages. Yale University Press, New Haven, CT, pp. 37–56.

Echer, E., 2004. Multi-resolution analysis of global total ozone column during 1979–1992 Nimbus-7 TOMS period. Annales Geophysicae 22, 1487–1493.

Echer, E., Rigozo, N.R., Souza Echer, M.P., Vieira, L.E.A., Nordemann, D.J.R., 2004. Reconstruction of the *aa* index on the basis of spectral characteristics. Geofisica Internacional 43, 103–111.

Eddy, J.A., 1976. The Maunder minimum. Science 192, 1189–1202.

Foukal, P., 1990. The variable sun. Scientific American 262, 34–41.

Fritts, H.C., 1976. Tree Ring and Climate. Academic Press Inc., London.

Graf, W., Oerter, H., Reinwarth, O., Stichler, W., Wilhelms, F., Miller, H., Mulvaney, R., 2002. Stable-isotope records from Dronning Maud Land, Antarctica. Annals of Glaciology 35, 195–201.

Haigh, J.D., 2003. The effects of solar variability on the Earth's climate. Philosophical Transactions of the Royal Society 361, 95–111.

Harrison, R.G., Carslaw, K.S., 2003. Ion–aerosol–cloud processes in the lower atmosphere. Reviews in Geophysics 41 (3), 1012.

Hudson, H.S., 1988. Observed variability of the solar luminosity. Annual Review of Astronomy and Astrophysics 26, 473–507.

Jackman, C.H., DeLand, M.T., Labow, G.J., Fleming, E.L., Weisenstein, D.K., Ko, M.K.W., Sinnhuber, M., Russell, J.M., 2005. Neutral atmospheric influences of the solar proton events in October–November 2003. Journal of Geophysical Research 110, A09S27.

Johnsen, S.J., Dansgaard, W., Clausen, H.B., Langway, C.C., 1970. Climatic oscillations 1200–2000 AD. Nature 277, 482–483.

Kumar, P., Foufoula-Georgiou, E., 1997. Wavelet analysis for geophysical applications. Reviews in Geophysics 35, 385–412.

Lean, J., Rind, D., 1994. Solar variability: implications for global change. EOS 75, 1–7.

Lean, J., Rind, D., 2001. Earth's response to a variable Sun. Science 292, 234–236.

Marsh, N., Svensmark, H., 2000. Cosmic rays, clouds, and climate. Space Science Reviews 94, 215–230.

Nordemann, D.J.R., Rigozo, N.R., Faria, H.H., 2005. Solar activity and El-Niño signals observed in Brazil and Chile tree ring records. Advances in Space Research 35, 891–896.

Percival, D.B., Walden, A.T., 2000. Wavelet Methods for Time Series Analysis. Cambridge University Press, Cambridge.

Peristykh, A.N., Damon, P.E., 1998. Modulation of atmospheric ^{14}C concentration by solar wind and irradiance components of Hale and Schwabe solar cycles. Solar Physics 177, 343–355.

Raspopov, O.M., Dergachev, V.A., Kolström, T., 2004. Periodicity of climate conditions and solar variability derived from dendrochronological and other palaeoclimatic data in high latitudes. Palaeogeography, Palaeoclimatology, Palaeoecology 209, 127–139.

Rigozo, N.R., Echer, E., Vieira, L.E.A., Nordemann, D.J.R., 2001. Reconstruction of Wolf sunspot number on the basis of spectral characteristics and estimates of associated radio flux and solar wind parameters for the last millennium. Solar Physics 203, 179–191.

Rigozo, N.R., Nordemann, D.J.R., 1998. Análise por regressão iterativa de periodicidades em series temporais de registros geofísicos. Revista Brasileira de Geofísica 16, 149–157.

Rigozo, N.R., Nordemann, D.J.R., Silva, H.E., Souza Echer, M.P., Echer, E., Prestes, A., 2006. Spectral analysis in tree ring width time series from Chile (1587–1994 A.D.). Trends in Applied Sciences Research 1, 73–78.

Solanki, S.K., Krivova, N.A., 2003. Can solar variability explain global warming since 1970? Journal of Geophysical Research 108 (A5), 1200.

Svensmark, H., Friis Christensen, E., 1997. Variation of cosmic ray flux and global cloud coverage—a missing link in solar–climate relationships. Journal of Atmospheric and Solar-Terrestrial Physics 59, 1225–1232.

Thompson, L.G., Mosley-Thompson, E., Bolzan, J.F., Koci, B.R., 1985. A 1500 year record of tropical precipitation recorded in ice cores from the Quelccaya Ice Cap, Peru. Science 229 (4717), 971–973.

Torrence, C., Compo, G.P., 1998. A practical guide to wavelet analysis. Bulletin of the American Meteorological Society 79, 61–78.

Vieira, L.E.A., da Silva, L.A., 2006. Geomagnetic modulation of clouds effects in the Southern Hemisphere Magnetic Anomaly through lower atmosphere cosmic ray effects. Geophysical Research Letters 33, L14802.

Wilson, R.C., Hudson, H.S., 1988. Sun luminosity variations in solar cycle 21. Nature 332, 810–812.

Wolberg, J.R., 1967. Prediction Analysis. D. Van Nostrand.